

Variational Quantum Algorithms for Dimensionality Reduction and Classification

Jin-Min Liang, Shu-Qian Shen,* Ming Li, and Lei Li

College of Science, China University of Petroleum, 266580 Qingdao, P.R. China

(Dated: June 14, 2022)

Dimensionality reduction and classification play an absolutely critical role in pattern recognition and machine learning. In this work, we present a quantum neighborhood preserving embedding and a quantum local discriminant embedding for dimensionality reduction and classification. These two algorithms have an exponential speedup over their respectively classical counterparts. Along the way, we propose a variational quantum generalized eigenvalue solver (VQGE) that finds the generalized eigenvalues and eigenvectors of a matrix pencil $(\mathcal{G}, \mathcal{S})$ with coherence time $O(1)$. We successfully conduct numerical experiment solving a problem size of $2^5 \times 2^5$. Moreover, our results offer two optional outputs with quantum or classical form, which can be directly applied in another quantum or classical machine learning process.

I. INTRODUCTION

Dimensionality reduction is significant to many algorithms in pattern recognition and machine learning. It is intuitively regarded as a process of projecting a high-dimensional data to a lower-dimensional data, which preserves some information of interest in the data set [1, 2]. The technique of dimensionality reduction has been variously applied in a wide range of topics such as regression [3], classification [4], feature selection [5].

Broadly speaking, all of these techniques were divided into two classes: linear and non-linear methods. Two most popular methods for linear dimensionality reduction are principal component analysis (PCA) and linear discriminant analysis (LDA). PCA is an orthogonal projection that minimizes the average projection cost defined as the mean squared distance between the data points and their projections [6]. The purpose of LDA is to maximize the between-class variance and minimize within-class scatter when the data has associated with class labels [7]. Perhaps, the most popular algorithm for non-linear dimensionality reduction is manifold learning [8]. The manifold learning algorithm aims to reconstruct an unknown nonlinear low-dimensional data manifold embedded in a high-dimensional space [9]. A number of algorithms have been proposed for manifold learning, including Laplacian eigenmap [10], locally linear embedding (LLE) [11], isomap [12]. Manifold learning has been successfully applied for video-to-video face recognition [13]. These nonlinear methods consider the structure of the manifold on which the data may possibly reside compared with Kernel-based techniques (e.g., Kernel PCA and Kernel LDA).

We are witnessing the development of quantum computation and quantum hardware. The discovery of quantum algorithm for factoring [14], database searching [15] and quantum matrix inverse [16] have shown that quantum algorithms have the capability of outperforming existed classical counterparts. Recently, quantum informa-

tion combines ideas from artificial intelligence and deep learning to form a new field: quantum machine learning (QML) [17]. For classification and regression, QML algorithms [18–22] also have shown advantages over their classical machine learning algorithms. However, much algorithms rely on the large-scale, fault-tolerate, universal quantum computer which may be achieved in the long future. Specifically, these algorithms will require enormous number of qubits and long depth of circuit to achieve quantum supremacy.

Fortunately, noisy intermediate-scale quantum (NISQ) devices is thought of as a significant step toward more powerful quantum computer [23]. This NISQ technology will be available in the near future. In this setting, hybrid algorithmic approaches demonstrate quantum supremacy in the NISQ era. This hybridization reduces the quantum resources including qubit counts, numbers of gates, circuit depth and numbers of measurements [24]. Variational hybrid quantum-classical algorithms aim to tackle complex problems using classical computer and near term quantum computer. The classical computer find the optimal parameters by minimizing the expectation value of objective function which is calculated entirely on the quantum computer.

The first class variational quantum algorithms have been proposed for preparing the ground state of a Hamiltonian [25]. For a Hamiltonian \mathcal{H} which is too large to diagonalize, one can approximate the ground state of the given Hamiltonian using the Rayleigh-Ritz variational method. After parameterizing the trial quantum states, one can perform a optimization subroutine to find the optimal state by tuning the optimal parameter. Variational method also is applied to obtain the excited state of a Hamiltonian [26, 27] and diagonalize a quantum state [24]. Another class hybrid algorithms is designed to find application in machine learning including the quantum approximate optimization algorithm (QAOA) [28], variational quantum algorithms for nonlinear partial differential equations [29] and linear systems of equations [30–33].

Inspired by the significant advantage of quantum algorithms, some authors designed quantum algorithms to reduce the dimension of a large data set in high dimensional

* sqshen@upc.edu.cn.

space. Quantum principal component analysis (qPCA) [34] and quantum linear discriminant analysis (qLDA) [35] are two potential candidates capable of compressing high dimensional data set and reducing the runtime to be logarithmic in the number of input vectors and their dimensions. These two protocols yield mappings for linear dimensionality reduction and obtain the projected vectors with only quantum form. Thus, a complicated quantum tomography [36] is needed if one would like to know all information of the projected vectors.

Motivated by manifold learning and quantum computation, one natural question arises of whether there have a quantum algorithm for dimensionality reduction and pattern classification, and in which preserves the local structure of original data space. To tackle this issue, we present two variational quantum algorithms. First one is quantum neighborhood preserving embedding (qNPE) which defines a map both on the training set and test set. The core of qNPE is a variational quantum generalized eigensolver (VQGE) based on Rayleigh quotient, a variant of quantum variational eigenvalue solver (QVE) [25], to prepare the generalized eigenpair (λ, x) of the generalized eigenvalue problem $Ax = \lambda Bx$. Based on the presented VQGE, we propose a quantum version of local discriminant embedding [37] for pattern classification on high-dimensional data. We show that these two algorithms achieve an exponential speedup over their classical counterparts.

The organization of the paper is as follows. In Section II, we give a quantum neighborhood preserving embedding (qNPE) for dimensionality reduction. The numerical experiments are conducted using 5-qubits to demonstrate the correctness of VQGE in subsection E of Section II. In Section III, we introduce the quantum local discriminant embedding (qLDE) in detail for classification problem. A summary and discussion are included in Section IV.

II. QUANTUM NEIGHBORHOOD PRESERVING EMBEDDING

Local linear embedding (LLE) [11] is an unsupervised method for nonlinear dimensionality reduction but it does not evaluate the maps on novel testing data points [38]. Neighborhood preserving embedding (NPE) is thought of as a linear approximation to the LLE algorithm [38]. NPE tries to find a projection suiting for the training set and testing set. Different from other linear dimensional reduction methods (PCA and LDA) which aim at maintaining the global Euclidean structure, NPE preserves the local manifold structure of data space. We assume that the regions will appear to be locally linear when the size of neighborhood is small and the manifold is sufficiently smooth. Experiments on face recognition have been conducted to demonstrate the effectiveness of NPE [38]. Here, we introduce a quantum neighborhood preserving embedding (qNPE). Given a set of

points $\{x_i\}_{i=0}^{M-1} \in \mathcal{M}$ and \mathcal{M} is a nonlinear manifold embedded in a D -dimensional real space \mathcal{R}^D , our qNPE attempts to retain the neighborhood structure of the manifold by representing x_i as a convex combination of its nearest neighbors. In particular, qNPE finds a transformation matrix A that maps these M points and test point x_{test} into a set of points $y_0, y_1, \dots, y_{M-1}, y_{test} \in \mathcal{R}^d$ in a lower-dimensional manifold space, where $y_i = A^\dagger x_i$, $y_{test} = A^\dagger x_{test}$, and the superscript \dagger denotes the conjugate transpose.

In the quantum setting, a quantum state preparation routine is necessary to construct the quantum states $\{|x_i\rangle\}_{i=0}^{M-1}$ corresponding to vectors $\{x_i\}_{i=0}^{M-1}$. Assume that we are given oracles for data set $\{x_i | x_i \in \mathcal{R}^D\}_{i=0}^{M-1}$ that return quantum states $\{|x_i\rangle\}_{i=0}^{M-1}$. Mathematically, an arbitrary D -dimensional vector $\vec{x}_i = \{x_{i0}, x_{i1}, \dots, x_{i(D-1)}\}$ is encoded into the D amplitudes $x_{i0}, x_{i1}, \dots, x_{i(D-1)}$ of an $O(\log D)$ -qubits quantum system, $|x_i\rangle = \sum_{j=0}^{D-1} x_{ij} |j\rangle$, where $\{|j\rangle\}$ is the computational basis [39].

A. Find the K -nearest neighbors

The first step of qNPE is the construction of a neighborhood graph according to the given data set. The construction of an adjacency graph G with M nodes relies on the K nearest neighbors of x_i . If x_j is one of the K nearest neighbors of x_i , then a directed edge will be drawn from the i th node to the j th node; otherwise, there is no edge. To preserve the local structure of the data set, we firstly develop an algorithm (Algorithm 1) to search the K nearest neighbors of point x_i .

Some notations are needed to understand Algorithm 1. Let $\{f(i) | i \in [0, 1, \dots, M-1]\}$ be an unsorted table of M items. We would like to find K indexes set $\mathcal{N} = \{j_1, j_2, \dots, j_K\}$ of the element such that $f(j_1) \leq f(j_2) \leq \dots \leq f(j_K) \leq f(j)$ where $\{j | j \in [0, 1, \dots, M-1]\}$ and $j \notin \mathcal{N}$. We call it quantum K nearest neighbors search which is a direct generalization of the quantum algorithm for finding the minimum [40]. One of our results is the following theorem.

Theorem 1. For a given quantum state set $\{|x_i\rangle\}_{i=0}^{M-1}$, ϵ denotes the estimation error of the inner product. Let $[0, 1, \dots, M-1]$ be an unsorted database of M items, each holding an inner product value. Algorithm 1 finds all lower K indexes with probability at least $\frac{1}{2}$ in runtime

$$O\left(\frac{M(M-1)}{2} \epsilon^{-1} \log D\right),$$

with query complexity $O(KM\sqrt{M})$.

Proof. Quantum K nearest neighbors search tries to find the K lower values of a unsorted data set. In step 1, given a state set

$$\{|x_i\rangle = \sum_{j=0}^{D-1} x_{ij} |j\rangle\}_{i=0}^{M-1},$$

we firstly estimate the square of inner product $|\langle x_i | x_k \rangle|^2$ over all data points for $i, k = 0, 1, \dots, M-1$ via swap test each running in times $O(\epsilon^{-1} \log D)$ with a given tolerate error ϵ [41]. The number of performing swap test is

$$T_{\text{swap}} = \sum_{i=0}^{M-1} i = \frac{M(M-1)}{2}.$$

Thus, the overall runtime of estimating square of inner product is $O(\frac{M(M-1)}{2} \epsilon^{-1} \log D)$.

In steps 2-4, we find K lower index set \mathcal{N} of one point $|x_i\rangle$. By adjusting $s = s - 1$, the index set T_s deletes one element every times. We repeat K times on the updated index set T_s to obtain the K lower index \mathcal{N} mapping to K smallest values. Durr et al. [40] have shown the query complexity of finding the minimum value is $O(\sqrt{M})$. In our algorithm, the query complexity of finding K nearest neighbors of one state $|x_i\rangle$ is

$$O\left(\sum_{k=1}^K \sqrt{M - (k-1)}\right) < O\left(K\sqrt{M}\right), \quad (1)$$

which has an upper bound $O(K\sqrt{M})$. Thus, the overall query complexity of traversal all quantum state set have an upper bound $Q = O(KM\sqrt{M})$. If we implement the entire algorithm on a classical computer, the time complexity requires exponential large $O(\frac{MD(M-1)}{2})$ with D and the query complexity is $O(KM^2)$. Obviously, the quantum K nearest neighbours search achieves an exponential speedup in the dimensionality of quantum states. ■

Algorithm 1: Quantum K nearest neighbors search

step 1: Estimate the overall square of inner product value via swap test with error at most ϵ in time $O(\frac{M(M-1)}{2} \epsilon^{-1} \log D)$.

Repeat the following steps K times:

step 2: Define an index set $T_s = [0, 1, \dots, s-1]$ where s is initialized as M .

step 3: Apply the minimum searching algorithm [40] and output a minimum index j in runtime $O(\sqrt{M})$ with probability at least $\frac{1}{2}$.

step 4: Reset $s = s - 1$.

Outputs: $\mathcal{N} = \{j_1, j_2, \dots, j_K\}$.

The query complexity of the presented algorithm can be further reduced to $O(M\sqrt{KM})$ using the idea of [42, 43]. Durr et al. [42] transformed the problem of finding d smallest values to find the position of the d zeros in the matrix consisting of boolean matrices with a single 0 in every row, which can be seen as a part of graph algorithm. Different from [42], Miyamoto and Iwamura [43] firstly found a good threshold by quantum counting and then values of all d indices are found via amplitude amplification. The values of all d indices are less than the value of the threshold index.

In summary, Algorithm 1 finds the K nearest neighbors $\mathcal{N}_i = \{x_0^i, x_1^i, \dots, x_{K-1}^i\}$ of quantum state $|x_i\rangle$ [44]. The presented algorithm is based on two algorithms: finding minimum and swap test. Firstly, we re-formulate the algorithm for finding K indices by updating the search set. Secondly, we explicitly analyse the time complexity and query complexity.

For implementation of the quantum K nearest neighbours search, only one free parameter, K , is taken into account. The threshold K affects the performance of qNPE. Specifically, it remains unclear how to select the parameter K in a principled manner. The qNPE will lose its nonlinear character and behave like traditional PCA if K is too large. In this case, the entire data space is seen as a local neighbourhood. In particular, if the threshold K is bigger than the dimension of data point, the loss function (2) described in subsection B will have infinite solutions and the optimal question will be irregular.

B. Obtain the weight matrix

Let W denote the weight matrix with element ω_j^i having the weight of the edge from node i to node j , and 0 if there is no such edge. For maintaining the local structure of the adjacency graph, we assume each data node can be approximated by the linear combination of its local neighbor nodes. It is the weight matrix that characters the relationship between the data points. The weights can be calculated by the following convex optimization problem,

$$\begin{aligned} \min \quad & \Phi(\omega_j^i) = \sum_{i=0}^{M-1} \|x_i - \sum_{j=0}^{K-1} \omega_j^i x_j^i\|^2 \\ \text{s.t.} \quad & \sum_{j=0}^{K-1} \omega_j^i = 1, i = 0, 1, \dots, M-1. \end{aligned} \quad (2)$$

Using the Lagrange multiplier to enforce the constraint condition $\sum_j \omega_j^i = 1$, the optimal weights are given by:

$$\omega_i = (\omega_1^i, \omega_2^i, \dots, \omega_K^i)^\dagger = \frac{G_i^{-1} \vec{1}}{\vec{1}^\dagger G_i^{-1} \vec{1}}, \quad (3)$$

where the covariance matrix is defined as $G_i = A_i^\dagger A_i$, and $A_i = X_i - N_i \in \mathcal{R}^{D \times K}$, $X_i = (x_i, x_i, \dots, x_i) \in \mathcal{R}^{D \times K}$, $\vec{1} = (1, 1, \dots, 1)^\dagger \in \mathcal{R}^K$, $N_i = (x_1^i, x_2^i, \dots, x_K^i) \in \mathcal{R}^{D \times K}$. The column vector $x_j^i \in \mathcal{N}_i$ of N_i represents the K -nearest data points close to the data point x_i . Each K -nearest data point in a D -dimensional real space \mathcal{R}^D . Our goal is to find weight quantum state $|\omega_i\rangle$ that satisfies

$$|\omega_i\rangle \propto \frac{|G_i^{-1} \vec{1}\rangle}{|\vec{1}^\dagger G_i^{-1} \vec{1}|}, \quad (4)$$

where $|G_i^{-1} \vec{1}\rangle = G_i^{-1} \vec{1} / \sqrt{\langle G_i^{-1} \vec{1} | G_i^{-1} \vec{1} \rangle}$. A key idea is to find the inverse of the matrix G with quantum technique.

In the following process, we make use of the matrix inverse algorithm shown in [16, 45] to prepare the quantum state $|\omega_i\rangle$. Let the singular value decomposition (SVD) of A_i be $A_i = U\Sigma V^\dagger = \sum_j \sigma_j^i |u_j^i\rangle\langle v_j^i|$, then the eigenvalue decomposition of covariance matrix G_i [46] is

$$G_i = \sum_{j=0}^{K-1} (\sigma_j^i)^2 |v_j^i\rangle\langle v_j^i|. \quad (5)$$

Thus, $|G_i^{-1}\vec{1}\rangle$ can be reexpressed as

$$|G_i^{-1}\vec{1}\rangle = \sqrt{\frac{1}{\sum_{j=0}^{K-1} |\beta_j^i|^2 / |\sigma_j^i|^4}} \sum_{j=0}^{K-1} \frac{\beta_j^i}{(\sigma_j^i)^2} |v_j^i\rangle, \quad (6)$$

where $\beta_j^i = \langle v_j^i | \vec{1} \rangle$. Assume that we are given a matrix oracle O_i which accesses the element A_{mn}^i of the matrix A_i :

$$|m\rangle|n\rangle|0\dots 0\rangle \mapsto |m\rangle|n\rangle|A_{mn}^i\rangle = |m\rangle|n\rangle|x_m^i - x_{nm}^i\rangle. \quad (7)$$

This oracle O_i can be provided by quantum random access memory (qRAM) using $O(KD)$ storage space in $O(\log^2 \max(K, D))$ operations [47]. With these preparations, we are able to efficiently simulate the unitary $U_i = e^{i\hat{A}_i}$ and prepare the weights state $|\omega_i\rangle$, where

$$\hat{A}_i = \begin{pmatrix} 0 & A_i \\ A_i^\dagger & 0 \end{pmatrix}.$$

To understand our algorithm quickly, we will give some details below. First of all, we perform quantum singular value decomposition (QSVD) of the matrix A_i on an initial state $|0\dots 0\rangle|\vec{1}\rangle$ to obtain the state $\sum_j \beta_j^i |\sigma_j^i\rangle|v_j^i\rangle$ containing singular values and right singular vectors of A_i . The first register is assigned to store the singular value and the second register to decompose $|\vec{1}\rangle$ in the space spanned by the right singular vectors of A_i . The vector $\vec{1} = (1, 1, \dots, 1)^\dagger$ corresponds to a quantum state $|\vec{1}\rangle = \frac{1}{\sqrt{K}}(1, 1, \dots, 1)^\dagger$ where K is a normalized constant. The quantum state $|\vec{1}\rangle = \sum_{j=0}^{K-1} \frac{1}{\sqrt{K}} |j\rangle$ can be easily prepared by applying $O(\log K)$ Hadamard gates on $O(\log K)$ qubits $|0^{\otimes \log K}\rangle$. Mathematically,

$$\begin{aligned} H^{\otimes \log K} |0^{\otimes \log K}\rangle &= \frac{1}{(\sqrt{2})^{\log K}} (|0\rangle + |1\rangle)^{\otimes \log K} \\ &= \frac{1}{\sqrt{K}} (|0\rangle + |1\rangle) \otimes \dots \otimes (|0\rangle + |1\rangle) \\ &= \frac{1}{\sqrt{K}} (|00\dots 0\rangle + |00\dots 1\rangle + \dots + |11\dots 1\rangle) \\ &= \sum_{j=0}^{K-1} \frac{1}{\sqrt{K}} |j\rangle. \end{aligned} \quad (8)$$

Now, we apply a unitary transformation taking σ_j^i to $\frac{C_i}{|\sigma_j^i|^2} \sigma_j^i$, where C_i is a normalized constant. Actually,

this rotation can be realized by applying $R_y(\sin^{-1} \frac{C_i}{|\sigma_j^i|^2})$ on the ancilla qubit $|0\rangle$,

$$\begin{aligned} &\sum_{j=0}^{K-1} \beta_j^i |\sigma_j^i\rangle |v_j^i\rangle |0\rangle \xrightarrow{R_y} \\ &\sum_{j=0}^{K-1} \beta_j^i |\sigma_j^i\rangle |v_j^i\rangle \left(\frac{C_i}{|\sigma_j^i|^2} |1\rangle + \sqrt{1 - \frac{C_i^2}{|\sigma_j^i|^4}} |0\rangle \right). \end{aligned} \quad (9)$$

Next, uncompute the singular value register and measure the ancilla qubit to obtain 1. The system are left with a state proportional to

$$|\omega_i\rangle \propto \sqrt{\frac{1}{\sum_{j=0}^{K-1} |C_i \beta_j^i|^2 / |\sigma_j^i|^4}} \sum_{j=0}^{K-1} \frac{C_i \beta_j^i}{|\sigma_j^i|^2} |v_j^i\rangle. \quad (10)$$

Obviously, the weight states $\{|\omega_i\rangle\}_{i=0}^{M-1}$ can be prepared by repeating the above process M times separately with the number of Hadamard gates scaling as $O(M \log K)$. However, taking into account the extraction of embedding vectors requiring a reconstructed weight matrix, we introduce an improved approach which achieves a parallel speedup in the preparation of the weight matrix. We reconstruct the weight matrix $W = (|\omega_0\rangle, |\omega_1\rangle, \dots, |\omega_{M-1}\rangle)$ via preparing an entanglement state $|\psi_W\rangle = \sum_{i=0}^{M-1} |\omega_i\rangle|i\rangle$. Theorem 2 validates the gate resources can be further reduced.

Theorem 2. For a given quantum state set $\{|x_i\rangle\}_{i=0}^{M-1}$, the task of preparing $|\psi_W\rangle = \sum_{i=0}^{M-1} |\omega_i\rangle|i\rangle$ with error at most ϵ has runtime

$$T_W = O\left(\frac{\log^2(K+D)}{\epsilon^3} \sum_{i=0}^{M-1} \|A_i\|_{max}^2\right).$$

The required gate resources are $O(\log MK)$.

Proof. We add an ancilla M dimension system which determines the applied unitary operator. Given the initial state $|\vec{1}\rangle_1 |0^{\otimes \log K}\rangle_2 |0^{\otimes \log M}\rangle_3 |0\rangle_4$, where $|\vec{1}\rangle = \frac{1}{\sqrt{K}}(1, 1, \dots, 1)^\dagger$. The register 3 gives the number of data set. After performing $O(\log MK)$ Hadamard gates on registers 2 and 3, we apply the conditional Hamiltonian evolution $e^{i\hat{A}_i t} \otimes |i\rangle$ on state

$$|\vec{1}\rangle_1 \sum_{i=0}^{M-1} \sum_{j=0}^{K-1} |j\rangle_2 |i\rangle_3 |0\rangle_4,$$

which achieves the following transformation,

$$\begin{aligned} &|\vec{1}\rangle_1 \sum_{i=0}^{M-1} \sum_{j=0}^{K-1} |j\rangle_2 |i\rangle_3 |0\rangle_4 \mapsto \\ &|\vec{1}\rangle_1 \sum_{i=0}^{M-1} \sum_{j=0}^{K-1} (e^{i\hat{A}_i t} \otimes |i\rangle\langle i|) |j\rangle_2 |i\rangle_3 |0\rangle_4 \\ &= \sum_{i=0}^{M-1} \sum_{j=0}^{K-1} |\sigma_j^i\rangle_1 |v_j^i\rangle_2 |i\rangle_3 |0\rangle_4. \end{aligned} \quad (11)$$

And then rotate the singular value by applying $R_y(\sin^{-1} \frac{C_i}{|\sigma_j^i|^2})$ on the ancilla qubit $|0\rangle_4$. The system state is

$$\sum_{i=0}^{M-1} \sum_{j=0}^{K-1} |\sigma_j^i\rangle_1 |v_j^i\rangle_2 |i\rangle_3 \left(\sqrt{1 - \frac{|C_i \beta_j^i|^2}{|\sigma_j^i|^4}} |0\rangle_4 + \frac{C_i \beta_j^i}{|\sigma_j^i|^2} |1\rangle_4 \right). \quad (12)$$

Finally, uncompute the first register and measure the fourth register to see 1, we obtain the state

$$\sum_{i=0}^{M-1} \sqrt{\frac{1}{\sum_{j=1}^K |C_i \beta_j^i|^2 / |\sigma_j^i|^4}} \sum_{j=0}^{K-1} \frac{C_i \beta_j^i}{|\sigma_j^i|^2} |v_j^i\rangle |i\rangle \quad (13)$$

which is proportional to the entangled state $\sum_{i=0}^{M-1} |\omega_i\rangle |i\rangle$.

The runtime of preparing the state $\sum_{i=0}^{M-1} |\omega_i\rangle |i\rangle$ is dominated by the quantum singular value estimation of $A_i \in \mathcal{R}^{D \times K}$. In the process, we consider an extended matrix $\hat{A}_i \in \mathcal{R}^{(K+D) \times (K+D)}$ and obtain the eigenvalues of \hat{A}_i by performing quantum phase estimate. According to [45], we prepare the state $|\omega_i\rangle$ with accuracy ϵ in runtime $O(\|A_i\|_{max}^2 \log^2(K+D)/\epsilon^3)$ where $\|A_i\|_{max}$ is the maximal absolute value of the matrix elements of A_i . Therefore, the entangled state $\sum_{i=0}^{M-1} |\omega_i\rangle |i\rangle$ is prepared in runtime

$$T_W = O\left(\frac{\log^2(K+D)}{\epsilon^3} \sum_{i=0}^{M-1} \|A_i\|_{max}^2\right). \quad (14)$$

Overall, only $O(\log MK)$ Hadamard gates is required along the way. Thus, the number of Hadamard gates is reduced to $O(\log MK)$ rather than $O(M \log K)$. ■

C. Variational quantum generalized eigenvalue solver

In this subsection, we obtain the projection matrix by solving the following cost function based on the locally linear reconstruction errors:

$$\Phi(y) = \sum_{i=0}^{M-1} \left(y_i - \sum_{j=0}^{K-1} \omega_j^i y_j \right)^2. \quad (15)$$

Here, the fixed weights ω_j^i characterize intrinsic geometric properties of each neighborhood. Each high-dimensional data $x_i \in \mathcal{R}^D$ is mapped to a low-dimensional data $y_i \in \mathcal{R}^d$. The embedding vector y_i is found by minimizing the cost function (15) over y_i . Following some matrix computation [11, 37], the cost function can be reduced to the generalized eigenvalue problem:

$$XQX^\dagger a = \lambda XX^\dagger a, \quad (16)$$

where $X = (x_0, x_1, \dots, x_{M-1})$, $Q = (I-W)^\dagger(I-W)$, $I = \text{diag}(1, \dots, 1)$. The detailed derivation is shown in Appendix A.

Algorithm 2: Variational quantum generalized eigenvalue solver

- step 1.* Design a quantum circuit, controlled by a set of experimental parameters $\{\theta_i\}$, which can prepare states $|\varphi\rangle = |\varphi(\{\theta_i\})\rangle$.
- step 2.* Define an objective function $f(\{\theta_i\}) = \frac{\langle \varphi | \mathcal{H}_G | \varphi \rangle}{\langle \varphi | \mathcal{H}_S | \varphi \rangle}$ which f maps parameters to a Rayleigh quotient of $|\varphi\rangle$ if $\langle \varphi | \mathcal{H}_S | \varphi \rangle \neq 0$.
- step 3.* Find all the generalized eigenvalues and corresponding generalized eigenstates.
- (a) Compute the expectation $\langle \mathcal{H}_{G(S),1} \rangle, \langle \mathcal{H}_{G(S),2} \rangle, \dots$, on $|\varphi_n\rangle = |\varphi_n(\{\theta_i\})\rangle$ for all terms of $\mathcal{H}_{G(S)}$ by quantum expectation estimation [25], which n denotes the iteration times of repeating Step 3.
- (b) Sum these values with appropriate weights, $h_{G(S)}$, to obtain

$$f_n = \frac{\langle \varphi_n | \mathcal{H}_G | \varphi_n \rangle}{\langle \varphi_n | \mathcal{H}_S | \varphi_n \rangle}.$$

- (c) Apply the classical minimization algorithm (e.g. gradient descent) to minimize f_n and determine the new parameter $\{\theta_i^n\}$.
- (d) Using step 1 to generate the state $|\varphi_n\rangle$.
- step 4.* Update the Hamiltonian:
- (a) if \mathcal{H}_G commutes with \mathcal{H}_S , $\mathcal{H}_G = (\mathcal{H}_G - \tau \mathcal{H}_S)^2$, $\mathcal{H}_S = (\mathcal{H}_S)^2$, else go to (b).
- (b) $\mathcal{H}_G = \mathcal{H}_G - \tau \mathcal{H}_S$, $\mathcal{H}_S = \mathcal{H}_S$, where τ is a parameter.
- step 5.* Perform Step 3 for a searched parameter τ .
- Output:** eigenstates $|\varphi_1\rangle, |\varphi_2\rangle, \dots$ with eigenvalues $0 \neq \lambda_1 = f_1 \leq \lambda_2 = f_2 \leq \dots \leq \lambda_n = f_n$.
-

The generalized eigenvalue problem, $\mathcal{G}x = \lambda \mathcal{S}x$, is an important challenge in scientific and engineering applications. Although Cong and Duan [35] has presented a Hermitian chain product to solve the generalized eigenvalue problem by replacing \mathcal{S}^{-1} with $\mathcal{S}^{-1/2}$, the computation of matrix inverse is extremely difficult on classical computer. Alternatively, quantum phase estimation (QPE) is a better candidate, but the simulation of $e^{i\mathcal{S}^{-1}\mathcal{G}}$ remains a fundamental challenge. Even though one can efficiently perform QPE, it still requires fully coherent evolution. Due to the above circumstances, Theorem 3 gives a variational quantum generalized eigenvalue solver (VQGE) for solving the generalized eigenvalue problem. Like the variational quantum eigenvalue solver (VQE) [25], our VQGE can also be run on near-term noisy devices.

Theorem 3. For an Hermitian matrix pencil $(\mathcal{G}, \mathcal{S})$ with invertible matrix \mathcal{S} , let $\epsilon > 0$ be a precision parameter. Algorithm 2 has the coherence time $O(1)$ that outputs all generalized eigenstates of the following generalized eigenvalue problem:

$$\mathcal{G}|\varphi\rangle = \lambda \mathcal{S}|\varphi\rangle,$$

requiring $O(1/\epsilon^2)$ repetitions, where $\mathcal{G}, \mathcal{S} \in \mathcal{R}^{n \times n}$ and $|\varphi\rangle$ is the generalized eigenstate corresponding to the generalized eigenvalue λ .

Proof. We first briefly review the subroutine quantum

expectation estimation (QEE) [25] in step 2. The QEE algorithm calculates the expectation value of a given Hamiltonian \mathcal{H} for a quantum state $|\varphi\rangle$. Any Hamiltonian can be rewritten as M terms [25, 48, 49], for real parameter $h_{12\dots}^{ij\dots}$

$$\begin{aligned}\mathcal{H} &= \mathcal{H}^1 + \mathcal{H}^2 + \dots \\ &= \sum_{i1} h_1^i \sigma_1^i + \sum_{ij12} h_{12}^{ij} \sigma_1^i \otimes \sigma_2^j + \dots, \quad (17)\end{aligned}$$

where Roman indices i, j, \dots denote the subsystem on which the operator acts, and 1, 2 identify the Pauli operator. Each subitem \mathcal{H}^m is a tensor product of Pauli operators. According to Eq. (17), the expectation value is

$$\begin{aligned}\langle \mathcal{H} \rangle &= \langle \mathcal{H}^1 \rangle + \langle \mathcal{H}^2 \rangle + \dots \\ &= \sum_{i1} h_1^i \langle \sigma_1^i \rangle + \sum_{ij12} h_{12}^{ij} \langle \sigma_1^i \otimes \sigma_2^j \rangle + \dots. \quad (18)\end{aligned}$$

As a result, each expectation $\langle \mathcal{H}^m \rangle$ is directly estimated using fermionic simulations [50] or statistical sampling [51].

In step 1, given a series of parameter vectors θ , the quantum circuit U is defined as

$$U(\theta) = U_L(\theta_L)U_{L-1}(\theta_{L-1})\dots U_1(\theta_1) \quad (19)$$

with L components. Mathematically, after preparing a N qubits initial quantum state $|0\rangle^{\otimes N}$, the generated quantum state is defined as

$$|\varphi\rangle = \Pi_{i=1}^L U_i(\theta_i)|0\rangle^{\otimes N}. \quad (20)$$

Note that the number of parameters and N are logarithmically proportional to the dimension of the generated state $|\varphi\rangle$ [52–54]. These parameterized quantum circuits has been shown significant potential in generative adversarial learning [55, 56] and quantum circuit Born machines [57].

In step 3, we show how to obtain the generalized eigenstate and corresponding generalized eigenvalue. Our results rely on the fact that the Rayleigh quotient [58]

$$R(|\varphi\rangle; \mathcal{G}, \mathcal{S}) = \frac{\langle \varphi | \mathcal{G} | \varphi \rangle}{\langle \varphi | \mathcal{S} | \varphi \rangle}, \langle \varphi | \mathcal{S} | \varphi \rangle \neq 0 \quad (21)$$

is stationary at $|\varphi\rangle \neq 0$ if and only if $(\mathcal{G} - \lambda\mathcal{S})|\varphi\rangle = 0$ for some scalar λ . Let $\mathcal{H}_\mathcal{G} = \mathcal{G}$ and $\mathcal{H}_\mathcal{S} = \mathcal{S}$ which also have the decomposition like (3). The first iteration obtains the generalized eigenstate with the lowest generalized eigenvalue.

To find overall eigenstates of $\mathcal{S}^{-1}\mathcal{G}$, we update the Hamiltonian $\mathcal{H}_\mathcal{G} = (\mathcal{H}_\mathcal{G} - \tau\mathcal{H}_\mathcal{S})^2$, $\mathcal{H}_\mathcal{S} = (\mathcal{H}_\mathcal{S})^2$, where τ is a parameter close to the energy of the generalized eigenstates, which turns the generalized eigenvalues into the ground state energy of updated Hamiltonian $(\mathcal{H}_\mathcal{G}, \mathcal{H}_\mathcal{S})$. The following derivation ensure this modification provides all generalized eigenvalues. For the generalized

eigenvalue problem $\mathcal{G}|\varphi\rangle = \lambda\mathcal{S}|\varphi\rangle$, the equation:

$$\begin{aligned}(\mathcal{H}_\mathcal{G} - \tau\mathcal{H}_\mathcal{S})^2|\varphi\rangle &= (\mathcal{H}_\mathcal{G}^2 + \tau^2\mathcal{H}_\mathcal{S}^2 - 2\tau\mathcal{H}_\mathcal{G}\mathcal{H}_\mathcal{S})|\varphi\rangle \\ &= (\lambda + \frac{\tau^2}{\lambda} - 2\tau)\mathcal{H}_\mathcal{G}\mathcal{H}_\mathcal{S}|\varphi\rangle \\ &= (\lambda - \tau)^2 \frac{1}{\lambda} \mathcal{H}_\mathcal{G}\mathcal{H}_\mathcal{S}|\varphi\rangle \\ &= (\lambda - \tau)^2 \mathcal{H}_\mathcal{S}^2|\varphi\rangle.\end{aligned} \quad (22)$$

The second equality uses the assumption that \mathcal{G} commutes with \mathcal{S} ($\mathcal{H}_\mathcal{G}\mathcal{H}_\mathcal{S} = \mathcal{H}_\mathcal{S}\mathcal{H}_\mathcal{G}$). Therefore, the Rayleigh quotient is

$$R_1 = \frac{\langle \varphi | (\mathcal{H}_\mathcal{G} - \tau\mathcal{H}_\mathcal{S})^2 | \varphi \rangle}{\langle \varphi | \mathcal{H}_\mathcal{S}^2 | \varphi \rangle} = (\lambda - \tau)^2. \quad (23)$$

Obviously, since the Rayleigh quotient is quadratic function of the variable τ , the ground generalized eigenstate of the updated Hamiltonian is found on the unique minimum point.

However, the above approach is useless when it is applied to the general situation such as $\mathcal{G}\mathcal{S} \neq \mathcal{S}\mathcal{G}$. An alternative approach now is presented. We update the Hamiltonian to the following form

$$\mathcal{H}'_\mathcal{G} = \mathcal{H}_\mathcal{G} - \tau\mathcal{H}_\mathcal{S}, \mathcal{H}'_\mathcal{S} = \mathcal{H}_\mathcal{S}.$$

The presented Hamiltonian induces a cost function

$$R'_1 = \left(\frac{\langle \varphi | (\mathcal{H}_\mathcal{G} - \tau\mathcal{H}_\mathcal{S}) | \varphi \rangle}{\langle \varphi | \mathcal{H}_\mathcal{S} | \varphi \rangle} \right)^2 = (\lambda - \tau)^2. \quad (24)$$

The classical computer then minimizes the function of (23), (24) and obtains the optimal parameter θ . The optimal values of (23), (24) are nearly zero for the suitable variable τ . For example, if the scanned τ is placed inside the energy gap, minimization of $R(|\varphi\rangle; (\mathcal{G} - \tau\mathcal{S})^2, \mathcal{S}^2)$ results in the generalized eigenstates energy of $\mathcal{H}_{\mathcal{S}^{-2}(\mathcal{G} - \tau\mathcal{S})^2}$. The searched method is similar to the idea of [59, 60]. Finally, we sort the generalized eigenvalues and output all eigenstates via the unitary circuit in step 1.

The time the quantum computer remain coherent is $O(1)$ which is determined by the extra depth of used circuit for preparing the parameterized state. If the desired error is at most ϵ , the cost of the expectation estimation of local Hamiltonian \mathcal{H}^m is $O(|\max\{h_{12\dots}^{ij\dots}\}|^2/\epsilon^2)$ repetitions of the preparation and measurement procedure. The overall generalized eigenstates can be prepared via n times queries for the parameter quantum circuit and M Hamiltonian items. Thus, we require

$$O(nM|\max\{h_{12\dots}^{ij\dots}\}|^2/\epsilon^2)$$

samples from the parameterized circuit with coherence time $O(1)$. ■

With the assistance of Theorem 3, only replacing \mathcal{G}, \mathcal{S} with XQX^\dagger and XX^\dagger can we find the d lower eigenstates

$\{|a_i\rangle\}_{i=0}^{d-1}$ as the column of the projection matrix A with runtime $O(1/\epsilon^2)$. Note that XQX^\dagger and XX^\dagger are positive definite matrix in $\mathcal{R}^{D \times D}$. One can firstly calculate these two Hermitian matrices by matrix multiplication algorithm [61]. Assuming that these two matrices can be regarded as raw-computable Hamiltonian, Berry et. al [48] have shown that XQX^\dagger and XX^\dagger may be decomposed as a sum of at most $O(6D^2)$ 1-sparse matrices each of which is efficiently simulated in $O(\log D)$ queries to the Hamiltonian.

D. Extract the lower-dimensional manifold

We now extract the low-dimension manifold based upon the projection matrix A . Firstly, a qRAM returns an equal superposition state $\frac{1}{\sqrt{d}} \sum_{i=0}^{d-1} |i\rangle$ with d qubits. This state prepares in quantum parallel the state $|A\rangle = \frac{1}{\sqrt{d}} \sum_{i=0}^{d-1} |a_i\rangle|i\rangle$ in $O(\log Dd)$ run time [47]. The state $|A\rangle$ encodes the information of the projection matrix A . The embedding state is given as:

$$\begin{aligned} |x_i\rangle &\mapsto |y_i\rangle = A^\dagger|x_i\rangle, \\ A &= (|a_0\rangle, |a_1\rangle, \dots, |a_{d-1}\rangle), \end{aligned} \quad (25)$$

where $|y_i\rangle$ is a d -dimensional vector and A is a $D \times d$ matrix. Our qNPE maps arbitrary high dimensional vector to a lower-dimensional vector. Thus if one is given a test vector $|x_{test}\rangle$, then the embedding vector is $|y_{test}\rangle = A^\dagger|x_{test}\rangle$.

Here, we propose two optional methods for the extraction of the embedding states. One of them is based on QSVD. Like [45], an extended matrix is considered as

$$\tilde{A} = \begin{pmatrix} 0 & A \\ A^\dagger & 0 \end{pmatrix}. \quad (26)$$

Assume that \tilde{A} has eigenvalue decomposition

$$\tilde{A} = \sum_j \sigma_j |\tilde{u}_+\rangle \langle \tilde{u}_+| - \sigma_j |\tilde{u}_-\rangle \langle \tilde{u}_-| \quad (27)$$

with singular value decomposition $A = \sum_j \sigma_j |u_j\rangle \langle v_j|$, where $|\tilde{u}_\pm\rangle = |u_j\rangle|0\rangle \pm |v_j\rangle|1\rangle$. We then perform QPE on the initial state $|0, x_i\rangle_1 |0, \dots, 0\rangle_2 |0\rangle_3$ and obtain a state

$$\sum_j \pm \alpha_j^\pm (-1)^{f_j} |\tilde{u}_\pm\rangle_1 \left| \frac{\sigma_j}{d+D} \right\rangle_2 |0\rangle_3, \quad (28)$$

where $\alpha_j^\pm = \pm \frac{\langle v_j|x_i\rangle}{\sqrt{2}}$. The third register indicates the flag qubit. If the eigenvalue is greater than the value of flag qubit 0, then $f_j = 0$, otherwise, $f_i = 1$. Performing a Pauli operator σ_z on the flag qubit and applying $R_y(2 \arcsin \sigma_i)$ on an ancilla qubit $|0\rangle$, we generate a state

$$\sum_j \alpha_j^+ |\tilde{u}_\pm\rangle_1 \left(\frac{\sigma_j}{d+D} |0\rangle + \sqrt{1 - \left(\frac{\sigma_j}{d+D}\right)^2} |1\rangle \right). \quad (29)$$

To this end, we project onto the $|u_j\rangle$ part and measure the final qubit to 0 resulting in a state

$$\sum_j \frac{\sigma_j}{d+D} \alpha_j^+ |u_j\rangle \propto U \sum V^\dagger |x_i\rangle = A^\dagger |x_i\rangle. \quad (30)$$

Repeating the above process M times, the embedding state $|y_0\rangle, |y_1\rangle, \dots, |y_{M-1}\rangle$ will be prepared with error ϵ in time $O(M \log^2(D+d)/\epsilon^3)$.

Alternatively, another approach is based on the well-known swap test [41]. Since the embedding low-dimensional data is

$$|y_i\rangle = A^\dagger|x_i\rangle = (\langle a_1|x_i\rangle, \langle a_2|x_i\rangle, \dots, \langle a_d|x_i\rangle)^\dagger, \quad (31)$$

we convert formula (25) into a computation of inner product item $\langle a_k|x_i\rangle$. The well-known swap test [41] calculates the square of the inner product by the expectation of operators. But here the magnitude and sign of these inner products are also required. Fortunately, the inner product can be estimated with $O(\log D)$ number of measurements [62, 63]. The embedding low-dimensional vector can be computed using resources scaling as $O(Md \log D)$. In summary, our algorithm outputs the embedding vectors with quantum (classical) form which can be directly applied in other quantum (classical) machine learning process.

E. Numerical simulations and performance analysis

In this subsection, we present a numerical experiment to simulate the proposed VQGE. The source code and the selected parameters of our numerical experiment can be accessed from [64].

For the implementation, we consider the following two 32×32 matrices (using 5-qubits).

Example 1:

$$\begin{aligned} \mathcal{G}_1 &= \mathbf{1} + 0.2\sigma_1^1 \otimes \sigma_2^2 + 0.2\sigma_1^1, \\ \mathcal{S}_1 &= \mathbf{1} + 0.0741\sigma_1^1 \otimes \sigma_2^2 + 0.3939\sigma_1^1, \end{aligned} \quad (32)$$

which has four generalized eigenvalues $\lambda_1 = 0.7577, \lambda_2 = 0.9537, \lambda_3 = 1.1278, \lambda_4 = 1.4702$.

Example 2:

$$\begin{aligned} \mathcal{G}_2 &= \mathbf{1} + 0.2\sigma_1^1 \otimes \sigma_3^2 + 0.2\sigma_1^1 + 0.2\sigma_3^1, \\ \mathcal{S}_2 &= \mathbf{1} + 0.1741\sigma_1^1 \otimes \sigma_3^1 + 0.2981\sigma_1^1, \end{aligned} \quad (33)$$

where σ_i^j denotes the Pauli operator σ_i acts on the j th subsystem.

Example 2 gives a general case for $\mathcal{G}_2\mathcal{S}_2 \neq \mathcal{S}_2\mathcal{G}_2$ which also has four generalized eigenvalues $\lambda_1 = 0.7780, \lambda_2 = 0.7987, \lambda_3 = 1.2533, \lambda_4 = 1.2891$. Here, the parameterized state is generated via the unitary circuit $U(\vec{\theta})$:

$$\begin{aligned} |\varphi(\vec{\theta})\rangle &= U(\vec{\theta})|0\rangle^{\otimes 5} \\ &= R_y(\theta_5)R_y(\theta_4)R_y(\theta_3)R_y(\theta_2)R_y(\theta_1)|0\rangle^{\otimes 5} \\ &= \bigotimes_{k=1}^5 \left(\cos \frac{\theta_j}{2} |0\rangle + \sin \frac{\theta_j}{2} |1\rangle \right). \end{aligned} \quad (34)$$

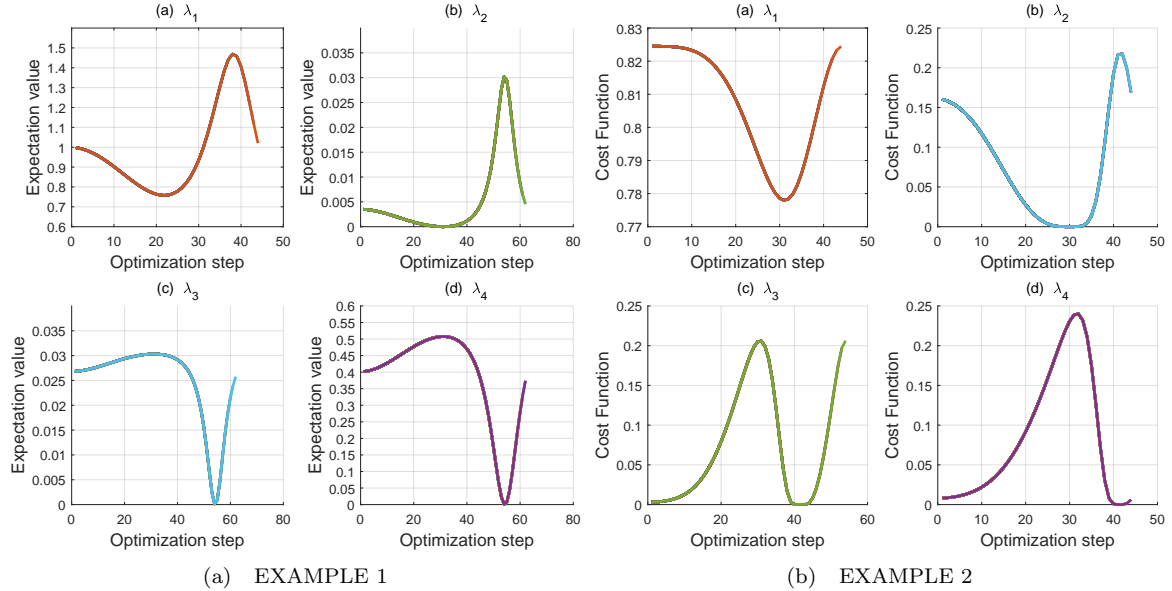


FIG. 1. Expectation values (cost function) versus number of optimization steps. The classical optimization algorithm performed is the fminsearch optimization based model order reduction. Notice that the minimal value of cost function in EXAMPLE 2 (c d) is reached about 40 steps.

The vector $\vec{\theta}$ is defined as $\vec{\theta} = (\theta_1, \theta_2, \dots, \theta_5)^\dagger$ and the rotation operator is $R_y = e^{-i\theta Y/2}$.

The experiments results of the VQGE implementation are shown in Fig. 1. As shown in Fig. 1(a), the expectation have a minimal value which implies the generalized ground state of a matrix pencil $(\mathcal{G}, \mathcal{S})$. In Fig. 1(b,c,d), we plot the expectation values (cost function) of the updated Hamiltonian with the optimization step. The generalized ground state of the updated Hamiltonian is always nearly zero. In these case, the generalized eigenvalues are reduced by the controlled parameter τ . Finally, once all optimal parameters are determined, we obtain the generalized eigenvalues via the expectation values of different Hamiltonian.

ITEMS	QUANTUM APPROACH				CLASSICAL APPROACH	
	TIME COMPLEXITY	QUERY COMPLEXITY	SAMPLE COMPLEXITY	COHERENCE TIME	TIME COMPLEXITY	QUERY COMPLEXITY
THEOREM 1	$\frac{M \cdot (M-1)}{2\epsilon} \log D$	$O(KM\sqrt{M})$	/	/	$O(KM(M-1)D)$	$O(KM^2)$
THEOREM 2	$O\left(\frac{\log^2(K+D)}{\epsilon^3} \sum_{i=0}^{M-1} \ A_i\ _{\max}\right)$	$O(\log KM)$	/	/	$O((K+D)^3M)$	
THEOREM 3	/	/	$O(1/\epsilon^2)$	$O(1)$	$O(n^2)$	

FIG. 2. The required resource complexity of quantum and classical methods.

Fig. 2 shows the required resources of quantum and classical methods. Classically, performing Theorem 2 takes $O((K+D)^3M)$. Complexity of the generalized eigenvalue problem is of order $O(n^3)$ on classical computation devices [65]. Since every step of qNPE has an exponential speedup, our qNPE absolutely outperforms classical NPE.

III. QUANTUM LOCAL DISCRIMINANT EMBEDDING

In this section, based on the variational quantum generalized eigenvalues (VQGE), we develop a quantum algorithm for pattern classification which preserves the local manifold. This algorithm is a quantum version of local discriminant embedding [37] (qLDE). The task is to classify a high-dimensional vector into one class, given M data points of the form $\{(x_i, y_i) : x_i \in \mathcal{R}^D, y_i \in \{1, 2, \dots, P\}\}_{i=0}^{M-1}$ where y_i depends on the class to which x_i belongs. Fig. 3 shows the expected effect of local discriminant embedding. After finding a associated submanifold of each class, the qLDE separates the embedded data points into a multi-class lower-dimensional Euclidean space.

First of all, one needs to construct two neighborhood graphs: the intrinsic graph G_w (within-class graph) and the penalty graph G_b (between-class graph). For each data point x_i , we define a subset $\mathcal{N}_{w,i,K}$ ($\mathcal{N}_{b,i,K'}$) which contains the K (K') neighbors having the same (different) class label with x_i . For graph G_w , we consider each pair of x_i and x_j with $y_i = y_j$. An edge is added between x_i and x_j if $x_j \in \mathcal{N}_{w,i,K}$. To construct G_b , likewise, we consider each pair of x_i and x_j with $y_i \neq y_j$. An edge is added if $x_j \in \mathcal{N}_{b,i,K'}$. Theorem 1 can help us to finish the construction of G_w and G_b by finding K (K') neighbors.

Next, we determine the weight matrix $W_{w(b)} = (W_{w(b),ij})$ of graph $G_w(G_b)$ by the following convex op-

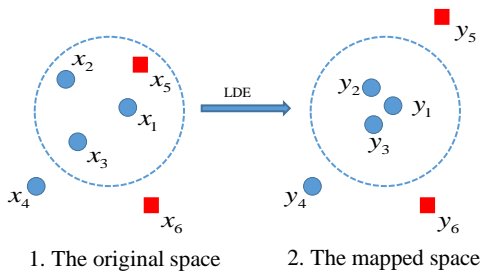


FIG. 3. The expected effect of LDE [66]. The point x_1 have four neighbors. The points with same color and shape belong to the same class. The within-class graph connects nearby points with the same label. The between-class graph connects nearby points with different labels. (b) After LDE, the local margins between different classes are maximized, and the distances between local homogeneous samples are minimized.

timization formulation:

$$\begin{aligned} \min \quad & \sum_i \|x_i - \sum_j W_{w(b),ij} x_j\|^2 \\ \text{s.t.} \quad & \sum_j W_{w(b),ij} = 1, i = 1, 2, \dots, M. \end{aligned} \quad (35)$$

Theorem 2 prepares two weight states

$$|\psi_{W_w}\rangle = \sum_{i=0}^{M-1} |\omega_{wi}\rangle |i\rangle, |\psi_{W_b}\rangle = \sum_{i=0}^{M-1} |\omega_{bi}\rangle |i\rangle,$$

with error at most ϵ in runtime

$$O\left(\frac{\log^2(K(K') + D)}{\epsilon^3} \sum_{i=0}^{M-1} \|A_i\|_{max}^2\right).$$

The required gate resource count is $O(\log MK(K'))$.

We next turn to find a matrix transform A that maximizes the local margins among different classes and pushes the homogenous samples closer to each other [66]. The overall process corresponds to the below mathematical formula:

$$\min_A \frac{1}{2} \sum_{ij} \|A^\dagger(x_i - x_j)\|^2 W_{w(b),ij}. \quad (36)$$

After simple matrix algebra (seeing details in [66]), the columns of optimal A are the generalized eigenvectors with the l largest eigenvalues in

$$T_b|a\rangle = \lambda T_w|a\rangle. \quad (37)$$

where $T_{w(b)} = X(I_{w(b)} - W_{w(b)})X^\dagger$, $X = (x_0, x_1, \dots, x_{M-1})$ and $I_{w(b)}$ is a diagonal matrix with $I_{w(b),ii} = \sum_j W_{w(b),ij}$. Then, we apply Theorem 3 to obtain the l generalized eigenvectors with l largest eigenvalues of (37).

Once we have learned the projection matrix A using qLDE, quantum nearest neighbor algorithm [19] is directly applied on multi-class classification tasks by computing the distance metrics between the test point $|y_{test}\rangle$ and other training points with a known class label. For example, for a given two clusters $\{U\}$ and $\{V\}$, if

$$\min_{u \in \{U\}} D(|y_{test}\rangle, |a\rangle) \leq \min_{v \in \{V\}} D(|y_{test}\rangle, |b\rangle), \quad (38)$$

then we can assign $|y_{test}\rangle$ to cluster class $\{U\}$, where D denotes the trace distance. The classification performance show exponential reductions with classical methods [19].

IV. CONCLUSIONS AND DISCUSSION

In conclusion, this work presented qNPE and qLDE for dimensionality reduction and classification. Both of them preserve the local structure of the manifold space in the process of dimensionality reduction. We demonstrated that qNPE achieves an exponential advantage over the classical case since every steps of qNPE have an exponential speedup. The performance of qLDE on classification tasks is also competitive with classical analog.

Along the way, we developed two useful subroutines in machine learning and scientific computation. The first one is quantum K nearest neighborhood search which finds K lowest values in an unordered set with $O(K\sqrt{N})$ times. It may help us sort an unordered list with an upper bound $O(N\sqrt{N})$. Another subroutine is a variation hybrid quantum-classical algorithm for solving the generalized eigenvalue problem. In electronic structure calculations, for instance, the electron density can be computed by obtaining the eigenpairs (E_m, Ψ_m) of the Schrödinger-type eigenvalue problem $\mathcal{H}\Psi_m = E_m\mathcal{S}\Psi_m$ with different discrete energies E_m , where \mathcal{H} denotes the Hamiltonian matrix and \mathcal{S} is a symmetric positive matrix [67]. Our variational quantum generalized eigenvalue solver can obtain the eigenpairs (E_m, Ψ_m) in runtime $O(1/\epsilon^2)$ with error ϵ independent of the size of the Hamiltonian. In addition, our VQGE can also determine the ground state and other excited states of an updated Hamiltonian. The presented method does not use the Hamiltonian simulation, amplitude amplification and phase estimation. We have performed numerical experiments solving the generalized eigenvalues problems with size $2^5 \times 2^5$.

Furthermore, our results provided two different output forms considering further study purpose. The output may be quantum or classical form, depending on the computation of interest. The quantum form encodes the monolithic information to a quantum state while the classical form directly outputs a classical discrete vector by quantum technique. These two output forms can be embedded into other large scale quantum or classical machine learning algorithms.

Although we have presented two algorithms for dimensionality reduction and classification, some questions still

need further study. For example, how to construct the Hamiltonian $X^\dagger Q X (X^\dagger X)$ from the entanglement state

$$|\psi_W\rangle = \sum_{i=0}^{M-1} |\omega_i\rangle |i\rangle. \quad (39)$$

Finally, as the effect of artificial neural networks to the quantum many-body problem [68], it would be interesting to investigate if our algorithms can also reduce the exponential complexity of the many-body wave function down to a tractable computational form.

Acknowledgments The authors thank anonymous referees and editor for useful feedback on the manuscript. This work is supported by NSFC (11775306) and the Fundamental Research Funds for the Central Universities (18CX02035A, 18CX02023A, 19CX02050A).

Appendix A: The derivation of Eq. (16)

In Appendix A, we give a detailed derivation of (16). The method can be found in the paper [38].

The cost function is

$$\Phi(y) = \sum_i \left(y_i - \sum_j \omega_j^i y_j \right)^2. \quad (A1)$$

The fixed weights ω_j^i characterize intrinsic geometric properties of each neighborhood. Each high-dimensional data $x_i \in \mathcal{R}^D$ is mapped to a low-dimensional data $y_i \in \mathcal{R}^d$. The weight matrix $W = (\omega_j^i)_{i,j=0}^{M-1}$ is an $M \times M$ sparse matrix. Suppose the transformation is linear ($y^\dagger = a^\dagger X$), where the i -th column vector of X is

x_i . We define

$$z_i = y_i - \sum_j \omega_j^i y_j. \quad (A2)$$

This equation can be rewritten as the vector form

$$z = y - W y = (I - W)y. \quad (A3)$$

Thus, the (A1) turns to

$$\begin{aligned} \Phi(y) &= \sum_{i=0}^{M-1} z^\dagger z = y^\dagger (I - W^\dagger)(I - W)y \\ &= a^\dagger X (I - W^\dagger)(I - W) X^\dagger a = a^\dagger X Q X^\dagger a. \end{aligned} \quad (A4)$$

Obviously, the matrix $X Q X^\dagger$ is symmetric and semi-positive definite. To remove an arbitrary scaling factor, we impose a constrain

$$y^\dagger y = 1 \Rightarrow a^\dagger X X^\dagger a = 1. \quad (A5)$$

Finally, the minimization problem reduces to

$$\begin{aligned} \arg \min_a \quad & a^\dagger X Q X^\dagger a \\ \text{s.t.} \quad & a^\dagger X X^\dagger a = 1. \end{aligned} \quad (A6)$$

Using the Lagrange multipliers and setting the derivative to zero, we can obtain the transformation vector a by the following generalized eigenvalues problem

$$X Q X^\dagger a = \lambda X X^\dagger a. \quad (A7)$$

-
- [1] A. Sarveniazi, *Am. J. Comput. Math*, **4**, 55 (2014).
[2] C. O. S. Sorzano, J. Vargas, and A. P. Montano, *arXiv:1403.2877*.
[3] H. Hoffmann, S. Schaal, and S. Vijayakumar, *Neural Process Lett.* **29**, 109 (2009).
[4] M. Vlachos, C. Domeniconi, D. Gunopulos, G. Kollios, and N. Koudas, in *Proc. ACM Int. Conf. Knowl. Discovery Data Mining*, **645** (2002).
[5] B. Chizi and O. Maimon, in *Data mining and knowledge discovery handbook*, **83** (2010).
[6] K. Pearson, *The London, Edinburgh and Dublin Philosophical Magazine and Journal of Science, Sixth Series*, **2**, 559 (1901).
[7] K. Fukunaga, *Introduction to Statistical Pattern Recognition* (Academic Press, New York, 1972).
[8] L. Cayton, *Univ. of California at San Diego Tech. Rep.* **12**, 1 (2005).
[9] A. J. Izenman, *Comput. Stat.* **4**, 439 (2012).
[10] M. Belkin and P. Niyogi, in *Proceedings of the 14th International Conference on Neural Information Processing Systems: Natural and Synthetic* (MIT Press, Cambridge, 2001), Vol. 14, pp. 585-591.
[11] S. T. Roweis and L. K. Saul, *Science* **290**, 2323 (2000).
[12] J. B. Tenenbaum, V. de Silva, and J. C. Langford, *Science* **290**, 2319 (2000).
[13] A. Hadid and M. Pietikainen. *European Workshop on Biometrics and Identity Management*. Springer, Berlin, Heidelberg, 2009.
[14] P. Shor, in *Symposium on Foundations of Computer Science* (IEEE, Piscataway, NJ, 1994), pp. 124-134.
[15] L. K. Grover, *Phys. Rev. Lett.* **79**, 325 (1997).
[16] A. W. Harrow, A. Hassidim, and S. Lloyd, *Phys. Rev. Lett.* **103**, 150502 (2009).
[17] J. Biamonte, P. Wittek, N. Pancotti, P. Rebentrost, N. Wiebe, and S. Lloyd, *Nature* **549**, 195 (2017).
[18] P. Rebentrost, M. Mohseni, and S. Lloyd, *Phys. Rev. Lett.* **113**, 130503 (2014).
[19] N. Wiebe, A. Kapoor, and K. M. Svore, *Quantum Inf. Comput.* **15**, 316 (2015).
[20] M. Schuld, I. Sinayskiy, and F. Petruccione, *Phys. Rev. A* **94**, 022342 (2016).
[21] G. Wang, *Phys. Rev. A* **96**, 012335 (2017).
[22] E. Aimeur, G. Brassard, and S. Gambs, *Mach. Learn.* **90**, 261 (2013).

- [23] J. Preskill, *Quantum* **2**, 79 (2018).
- [24] R. LaRose, A. Tikku, É. O’Neil-Judy, L. Cincio, and P. J. Coles, *npj Quantum Inform.* **5**, 57 (2019).
- [25] A. Peruzzo, J. McClean, P. Shadbolt, M.-H. Yung, X.-Q. Zhou, P. J. Love, A. Aspuru-Guzik, and J. L. O’Brien, *Nat. Commun.* **5**, 4213 (2014).
- [26] O. Higgott, D. Wang, and S. Brierley, *Quantum* **3**, 156 (2019).
- [27] T. Jones, S. Endo, S. McArdle, X. Yuan, and S. C. Benjamin, *Phys. Rev. A* **99**, 062304 (2019).
- [28] E. Farhi, J. Goldstone, and S. Gutmann, [arXiv:1411.4028](https://arxiv.org/abs/1411.4028) (2014).
- [29] M. Lubasch, J. Joo, P. Moinier, M. Kiffner, D. Jaksch, [arXiv:1907.09032](https://arxiv.org/abs/1907.09032) (2019).
- [30] X. Xu, J. Sun, S. Endo, Y. Li, S. C. Benjamin, and X. Yuan, [arxiv:1909.03898](https://arxiv.org/abs/1909.03898) (2019).
- [31] D. An and L. Lin, [arXiv:1909.05500](https://arxiv.org/abs/1909.05500) (2019).
- [32] H.-Y. Huang, K. Bharti, P. Rebentrost, [arXiv:1909.07344](https://arxiv.org/abs/1909.07344) (2019).
- [33] C. Bravo-Prieto, R. LaRose, M. Cerezo, Y. Subasi, L. Cincio, and P. J. Coles, [arXiv:1909.05820](https://arxiv.org/abs/1909.05820) (2019).
- [34] S. Lloyd, M. Mohseni, and P. Rebentrost, *Nat. Phys.* **10**, 631 (2014).
- [35] I. Cong and L. Duan, *New J. Phys.* **18**, 073011 (2016).
- [36] M. A. Nielsen, I. L. Chuang, *Quantum Computation and Quantum Information* (Cambridge Univ. Press, 2000).
- [37] H.-T. Chen, H.-W. Chang, and T.-L. Liu, IEEE Computer Society Conference on Computer Vision and Pattern Recognition (2005).
- [38] X. He, D. Cai, S. Yan, and H. J. Zhang, In *Proceedings of the Tenth IEEE International Conference on Computer Vision*, pp 1208-1213, 2005.
- [39] M. Schuld, I. Sinayskiy, and F. Petruccione, *Phys. Rev. A* **94**, 022342 (2016).
- [40] C. Durr and P. Hoyer, [arXiv:1907.01414](https://arxiv.org/abs/1907.01414).
- [41] H. Buhrman, R. Cleve, J. Watrous, and R. de Wolf, *Phys. Rev. Lett.* **87**, 167902 (2001).
- [42] C. Durr, M. Heiligman, P. Hoyer, and M. Mhalla, *SIAM J. Comput.* **35**, 1310, (2006).
- [43] K. Miyamoto, M. Iwamura, and K. Kise, [arXiv:1907.03315](https://arxiv.org/abs/1907.03315) (2019).
- [44] The set \mathcal{N}_i contains K vector states which also reside in the M quantum states set.
- [45] P. Rebentrost, A. Steffens, I. Marvian, and S. Lloyd, *Phys. Rev. A* **97**, 012327 (2018).
- [46] Here, we decompose the covariance matrix G_i by the singular value decomposition of matrix A_i . In this situation, one can perform QSVD of A_i to obtain the corresponding singular value. Alternatively, one can directly apply quantum phase estimation of G_i . However, an extra computation expense of the elements of G_i is paid by matrix multiplication algorithm [61] on classical computer. Thus, our decomposition of covariance matrix G_i is a computationally-friendly scheme.
- [47] V. Giovannetti, S. Lloyd, and L. Maccone, *Phys. Rev. Lett.* **100**, 160501 (2008).
- [48] D. W. Berry, G. Ahokas, R. Cleve, and B. C. Sanders, *Commun. Math. Phys.* **270**, 359 (2007).
- [49] A. M. Childs and R. Kothari, in *Theory of Quantum Computation, Communication, and Cryptography: 5th Conference, TQC 2010, Leeds, UK, April 13-15, 2010, Revised Selected Papers*, edited by W. van Dam, V. M. Kendon, and S. Severini (Springer, Berlin, 2011), pp. 94C103.
- [50] G. Ortiz, J. E. Gubernatis, E. Knill, and R. Laflamme, *Phys. Rev. A* **64**, 022319 (2001).
- [51] J. Romero, R. Babbush, J. R. McClean, C. Hempel, P. J. Love, and A. Aspuru-Guzik, *Quantum Sci. Technol.* **4**, 014008 (2019).
- [52] A. Kandala, A. Mezzacapo, K. Temme, M. Takita, M. Brink, J. M. Chow, and J. M. Gambetta, *Nature* **549**, 242 (2017).
- [53] Y. Du, M.-H. Hsieh, T. Liu, and D. Tao, [arXiv:1810.11922](https://arxiv.org/abs/1810.11922).
- [54] K. Mitarai, M. Negoro, M. Kitagawa, and K. Fujii, *Phys. Rev. A* **98**, 032309 (2018).
- [55] S. Lloyd and C. Weedbrook, *Phys. Rev. Lett.* **121**, 040502 (2018).
- [56] P.-L. Dallaire-Demers and N. Killoran, *Phys. Rev. A* **98**, 012324 (2018).
- [57] J.-G. Liu and L. Wang, *Phys. Rev. A* **98**, 062324 (2018).
- [58] B. N. Parlett, *The Symmetric Eigenvalue Problem* (Society for Industrial and Applied Mathematics, Philadelphia, 1998).
- [59] Y. Shen, X. Zhang, S. Zhang, J.-N. Zhang, M.-H. Yung, and K. Kim, *Phys. Rev. A* **95**, 020501 (2017).
- [60] L.-W. Wang and A. Zunger, *J. Chem. Phys.* **100**, 2394 (1994).
- [61] D. Coppersmith and S. Winograd, *J. Symb. Comput.* **9**, 251 (1990).
- [62] N. Liu and P. Rebentrost, *Phys. Rev. A* **97**, 042315 (2018).
- [63] Z. Zhao, J. K. Fitzsimons, and J. F. Fitzsimons, *Phys. Rev. A* **99**, 052331 (2019).
- [64] VQGE source code. <https://github.com/jmliang24/VQGE-source-code-EXAMPLE1.git>.
- [65] G. H. Golub and C. F. Van Loan, *Matrix computations*, Vol. 3 (JHU Press, 2012).
- [66] F. Dornaika and A. Bosaghzadeh, *IEEE T. Cybern.* **43**, 921 (2013).
- [67] E. Polizzi, *Phys. Rev. B* **79**, 115112 (2009).
- [68] G. Carleo and M. Troyer, *Science* **355**, 602 (2017).